Functional Contacts between MPER and the Anti-HIV-1 Broadly Neutralizing Antibody 4E10 Extend into the Core of the Membrane

Rujas, Edurne
Biofisika Institute (CSIC, UPV/EHU) and Department of Biochemistry and Molecular Biology, University of the Basque Country | Department of Bioengineering, Graduate School of Engineering, The University of Tokyo

Insausti, Sara
Biofisika Institute (CSIC, UPV/EHU) and Department of Biochemistry and Molecular Biology, University of the Basque Country

Garcia-Porras, Miguel
Biofisika Institute (CSIC, UPV/EHU) and Department of Biochemistry and Molecular Biology, University of the Basque Country

Sánchez-Eugenia, Rubén
Biofisika Institute (CSIC, UPV/EHU) and Department of Biochemistry and Molecular Biology, University of the Basque Country

他

出版情報：Journal of molecular biology. 429 (8), pp.1213-1226, 2017-04-17. Academic Press
バージョン：
権利関係：

Functional contacts between MPER and the anti-HIV-1 broadly neutralizing antibody 4E10 extend into the core of the membrane.

Edurne Rujas[1,2], Sara Insausti[1], Miguel García-Porras[1], Rubén Sánchez-Eugenia[1], Kouhei Tsumoto[2], José L. Nieva[1*], Jose M. M. Caaveiro[2,3*]

[1]Biofisika Institute (CSIC, UPV/EHU) and Department of Biochemistry and Molecular Biology, University of the Basque Country, P.O. Box 644, Bilbao 48080, Spain. [2]Department of Bioengineering, Graduate School of Engineering, The University of Tokyo, Bunkyo-ku, Tokyo 113-8656, Japan, [3]Laboratory of Global Healthcare, School of Pharmaceutical Sciences, Kyushu University, 3-1-1 Maidashi, Higashi-Ku, Fukuoka 812-8582, Japan.

*Corresponding author: J.L.N.; Phone: +(34) 94-601-3353, FAX: +(34) 94-601-3360.

*Corresponding author: J.M.M.C.; Phone +(81) 9-2642-6617, FAX: +(81) 3-6409-2129.

ABSTRACT

The exceptional breadth of broadly neutralizing antibodies (bNAbs) against the membrane-proximal external region (MPER) of the transmembrane protein gp41 makes this class of antibodies an ideal model to design HIV vaccines. From a practical point of view, however, the preparation of vaccines eliciting bNAbs is still a major roadblock that limits their clinical application. Fresh mechanistic insights are necessary to develop more effective strategies. In particular, the function of the unusually long complementary determining region three of the heavy chain (CDRH3) of 4E10, an anti-MPER bNAb, is an open question that fascinates researchers in the field. Residues comprising the apex region are dispensable for engagement of the epitope in solution, still their single mutation profoundly impairs the neutralization capabilities of the antibody. Since this region is very hydrophobic, it has been proposed that the apex is essential for anchoring the antibody to the viral membrane where MPER resides. Herein we have critically examined this idea using structural, biophysical, biochemical, and cell-based approaches. Our results demonstrate that the apex region is not just a "greasy" spot merely increasing the affinity of the antibody for the membrane. We demonstrate the three-dimensional engagement of the apex region of the CDRH3 with the conglomerate of gp41 epitope and membrane lipids as a means of effective binding and neutralization of the virus. This mechanism of recognition suggests a standard route of antibody ontogeny. Therefore, we need to focus our efforts on recreating a more realistic MPER/lipid immunogen in order to generate more effective anti-HIV-1 vaccines.

Graphical Abstract

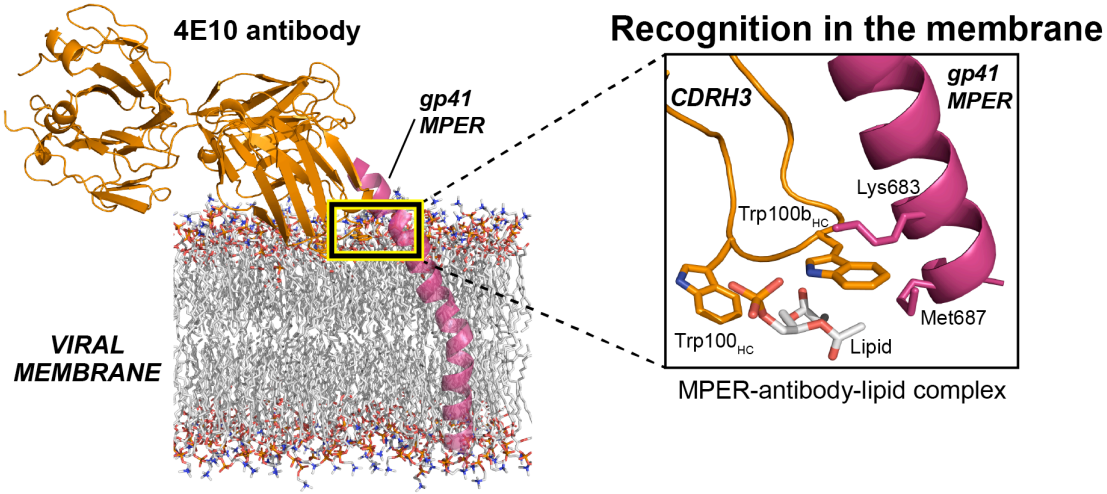

Highlights

- The hydrophobic apex of CDRH3 of 4E10 is critical for blocking HIV-1, but why?
- Hydrophobicity facilitates membrane binding but cannot explain neutralization potency
- The two tryptophan residues of the apex penetrate into the core of the lipid bilayer
- One of these tryptophan residues contacts the epitope in the interior of the membrane
- The mechanism revealed in this study may impact the design of anti-HIV-1 vaccines

Keywords: 4E10 antibody; antigen-antibody binding; protein-membrane interaction; vaccine development; complementary determining region, biomolecular recognition.

Abbreviations used: Broadly neutralizing antibodies, bNAbs; membrane-proximal external region, MPER; complementary determining region, CDR; virus-like, VL; transmembrane domain, TMD; wild-type, WT; pseudovirus particles (PsVs); dodecyl-phosphocholine, DPC; *p*-benzoylphenylalanine, *p*BPA; 4-chloro-7-nitrobenz-2-oxa-1,3-diazole, NBD; 1,2-dioleoyl-sn-glycerol-3-phosphoethanolamine-N-(lissamine rhodamine B sulfonyl), Rho-PE; 1,2-dioleoyl-*sn*-glycero-3-phosphocholine, DOPC; 1,2-dioleoyl-*sn*-glycero-3-phosphoethanolamine, DOPE; 1,2-dioleoyl-*sn*-glycero-3-phosphoserine, DOPS; sphingomyelin, SM; cholesterol, Chol; 1-palmitoyl-2-oleoyl-sn-glycero-3-phosphocholine, POPC; Large unilamellar vesicles, LUV.

INTRODUCTION

The broadly neutralizing anti-HIV-1 antibody 4E10 targets the highly conserved membrane-proximal external region (MPER) of the membrane protein gp41, exhibiting one of the greatest neutralization breadths described so far [1-3]. There is genuine interest to understand the molecular basis by which the antibody 4E10, and other broadly neutralizing antibodies (bNAbs), recognize such a broad repertoire of HIV-1 subtypes because this knowledge could translate into novel and more efficient vaccination strategies. In particular, previous studies made clear that hydrophobic and aromatic residues belonging to the apex of the heavy-chain complementarity determining region three (CDRH3) of 4E10 are critical for viral neutralization [4-6], although their mechanism of action at the molecular level is still awaiting clarification. Specially, it is unclear how these residues contribute to the recognition of the epitope in the context of the viral membrane where MPER resides. These questions are more relevant in view that the hydrophobic residues of the apex region of the CDRH3 remain in a conformation exposed towards the solvent, and not oriented towards the bound peptide as it could be expected from their critical role in the virus neutralization by the antibody [7-12]. In contrast, the functionally similar bNAb 10E8 positions the apex of the CDRH3 loop in close proximity to the MPER peptide [13,14] thus rationalizing its neutralization potency in terms of binding affinity to the epitope in membranes.

The unusual length and hydrophobicity of the CDRH3 is shared by both 4E10 and 10E8 antibodies, suggesting that the recognition mechanism of the MPER epitope in the environment of the viral membrane could be similar to each other. In the specific case of 4E10, the recognition of the epitope may be even preceded by the integration of the CDRH3 in the viral membrane, facilitating the reconfiguration of the CDRH3 apex with respect to the conformation observed in the crystal structure of complexes Fab-peptide [8,9,11]. In support of this hypothesis, a recent

crystallographic study evidenced that the presence of lipids triggers a conformational change of the CDRH3 of 4E10 facilitating the engagement of the full-length epitope by the antibody [10].

Herein we sought to determine two critical aspects, not addressed before, necessary for the functional engagement of 4E10 to the epitope in a membrane-mimicking environment. First, we investigated the molecular principles of the interaction of the CDRH3 of 4E10 with membranes, such as the partition of the antibody into proteoliposomes, the conformational change of CDRH3, and the formation of intermolecular contacts mediated by the apex of the CDRH3. Second, we evaluated the importance of these molecular contacts for the neutralization potency of the antibody. In particular, we monitored the physicochemical environment at two key positions of the apex of the CDRH3 ($Trp100_{HC}$ and $Trp100b_{HC}$) upon binding to membranes using a reporter probe. The proximity of these two locations of the CDRH3 of the antibody to the transmembrane domain (TMD) of the viral gp41 was assessed using a genetically encoded photoreactive amino acid. From these experiments, we inferred the relative orientation of the Trp residues with respect to the MPER/TMD region when inserted into the membrane.

Based on the data, we herein suggest that the apex of the CDRH3 loop fulfills at least two critical functions during viral neutralization: (i) to promote the partition of the antibody into the membrane, and (ii) to strengthen the antibody-epitope complex. The key residues governing the polyfunctionality of the apex are the two Trp residues there, in particular $Trp100b_{HC}$, which directly engages the epitope at the membrane interface stabilizing the antibody-antigen complex. These findings contribute to clarify the mechanism of viral neutralization by 4E10, inspiring the design of vaccines capable of inducing antibodies with 4E10-like neutralization breadth.

RESULTS

Molecular contribution of the apex region of the CDRH3 to the function of 4E10.

The ability of anti-MPER antibodies to neutralize HIV-1 has been correlated with the hydrophobicity at the apex of their unusually long CDRH3 loop [4,13,15]. Despite the fundamental role of those residues for viral neutralization, the molecular basis explaining their function is unknown. Two hypotheses have been proposed. One such models considers that the hydrophobic residues of the apex enhance the binding by the avidity-effect [16], whereas a second possibility considers that the apex region favors antibody pre-targeting to the viral membrane prior to fusion [5]. We believe that the CDRH3 loop mediates viral blocking beyond promoting the unspecific partitioning into the membrane, a hypothesis in agreement with the general basis of specificity in antibody-antigen binding [17]. To evidence the more active role of the CDRH3 apex beyond the merely unspecific hydrophobic effect, we generated several versions of 4E10 Fab differing in the composition and order of residues comprising the region ^{100}WGWL^{100c} and evaluated their hydrophobicity, partitioning into membranes, and neutralization potency (Fig. 1).

Interfacial hydrophobicity and sequence of the CDRH3 apex was altered employing four different approaches. First, one or both tryptophan residues of the apex were replaced with residues of different hydrophobicity (W100$_{HC}$C, W100b$_{HC}$C, W100$_{HC}$Y/W100b$_{HC}$Y, or W100$_{HC}$D/W100b$_{HC}$D). Second, the residue Leu100c$_{HC}$ of the CDRH3 apex was substituted with a tryptophan residue to render the mutant that we termed 3W, displaying greater interfacial hydrophobicity than wild-type Fab. Third, the residues of the apex of 4E10 were exchanged with the functional apex (^{106}LFGV^{109}) of the broadly neutralizing anti-MPER antibody 2F5 [15]. We employed the apex of the antibody 2F5 because it has an active role in mediating lipid binding and antibody neutralization without binding to MPER [15] in a similar manner to that proposed

for the 4E10 antibody. And fourth, "scrambled" mutants of the apex preserving the overall hydrophobicity and amino acid composition of the loop, but modifying the order of residues in the sequence were prepared (Scr-1; Scr-2, and Scr-3) (Fig. 1a).

The ability of the mutated Fabs to bind to the membrane was assessed by subjecting samples of Fab incubated with virus-like (VL) vesicles, mimicking the lipid composition of the viral membrane (see materials and methods), to a sucrose gradient (Fig. 1b). The partitioning of the Fab into membranes was qualitatively estimated from the co-localization of antibody and vesicles (fraction 4) as detected by western-blot and fluorescence, respectively. The hydrophobicity of the sequences examined were calculated using the Wimley and White hydrophobicity-at-interface scale [18]. By using the Wimley-White scale, the hydrophobicity can be quantified in terms of the free energy of transfer from bilayer interface to water (ΔG_{iwu}, also termed free energy of partitioning). The neutralization potency of the antibody was determined by using pseudovirus particles (PsVs) [11,14].

The hydrophobicity at the apex generally correlates positively with the partition of the antibody into the membrane, and with its neutralization potency (Fig. 1b,c), but there were also exceptions. Although the WT, Scr-1, Scr-2 and Scr-3 antibodies (dashed-box in Fig. 1c) all showed identical hydrophobicity and similar tendency to partition into membranes, they displayed a broad range of neutralization responses. Therefore, although the hydrophobicity of the CDRH3 at the apex region plays an important role in the function of 4E10, probably enhancing the binding of the antibody to the membrane, it is also important to maintain a specific sequence to maximize the potency of the antibody. These results suggest the existence of non-specific as well as specific interactions between antibody, epitope, and lipids at the membrane interface. In the following sections we sought to determine the spatial positions of the two largest

hydrophobic residues, Trp100$_{HC}$ and Trp100b$_{HC}$, during their association with epitope and lipids at the membrane interface, and their relative importance for the activity of the antibody.

Insertion of the apex into the membrane.

The results above, as well as previous mutational studies [4,5], clearly demonstrate that the presence of the apex of the CDRH3 is indispensable for the interaction with membranes. However, despite the high propensity of Trp residues to locate at the membrane interface, the relative position of the key Trp100b$_{HC}$ and Trp100$_{HC}$ residues in the membrane has not been elucidated. A recent study has suggested that the apex undergoes a conformational change in the presence of short acyl-chain lipids that form micelles [10]. However, it is still unclear whether the apex would insert into membrane bilayers as illustrated for the model in micelles (Fig. 2a), or would serve to partition into the membrane interface to merely increase the adherence to the surface of the membrane, first proposed based on crystal structures of Fab 4E10 in complex with short peptides [8,9].

To answer that question, flotation experiments were first conducted to ensure that comparable and efficient partitioning of 4E10 into vesicles occurs both in absence and presence of peptide (Fig. 2b). Next, we separately introduced the molecular sensor 4-chloro-7-nitrobenz-2-oxa-1,3-diazole (NBD) at the position of each Trp (100$_{HC}$ and 100b$_{HC}$) and monitored the changes of fluorescence in the presence of lipid vesicles (Fig. 2c,d). The observed shift of the emission maximum from 543 to 539 nm is suggestive of transfer of the NBD moiety from a high to a low polarity environment [19,20]. This change was accompanied by an increase of the fluorescence intensity. These results suggest that the positions 100$_{HC}$ and 100b$_{HC}$ of the CDRH3 spontaneously insert into the hydrophobic core of the bilayer.

The fluorescence intensity of the NBD moiety also increased, and the emission maximum decreased, upon incubation of the two NBD-labeled Fabs with liposomes decorated with increasing concentrations of the peptide MPER(671-690) (Fig. 2e,f). In addition, in all the fluorescence experiments carried out (with or without peptide) the changes of fluorescence are remarkably similar for the two positions examined. Collectively, these experiments demonstrated for the first time that the two Trp residues occupying these positions in the WT antibody insert into the membrane to a similar extent. They also prove that the antibody is capable to partition into vesicles with or without epitope present. In both circumstances, the apex region of the CDR-H3 inserts into the hydrophobic core of the lipid bilayer.

Proximity between the apex and MPER at interfaces.

We have recently identified the existence of non-covalent interactions between the apex residue Trp100b$_{HC}$ of the 10E8 antibody, and residues of gp41 fully embedded in the membrane [14]. These interactions strengthen the affinity of the antigen-antibody complex when the epitope is embedded in the membrane, increasing the inhibitory capabilities of the antibody. Taking into account that the Trp residues at the apex of the CDRH3 of 4E10 penetrate in the lipid membrane also in response to the epitope (Fig. 2e,f), we examined whether the apex of the CDRH3 may also interact with residues of the TMD of gp41. In order to verify this hypothesis, photo-cross-linking experiments with a genetically encoded unnatural amino acid were conducted. Positions 100$_{HC}$ and 100b$_{HC}$ of the CDRH3 (Fig. 3a) were substituted with the photoreactive amino acid *p*-benzoylphenylalanine (*p*BPA). This is a large unnatural amino acid possessing a rigid side-chain composed of two co-planar aromatic rings, and therefore showing certain similarities to a Trp residue (Fig. 3b), that reacts with neighboring aliphatic carbon atoms when activated with UV-

light. The resulting Fab mutants were irradiated with UV-light in the presence of peptides of various lengths, in some cases including residues of the TMD region (Fig. 3c).

When the photoreactive amino acid *p*BPA occupied the position $100b_{HC}$ of the Fab, the SDS-PAGE gel revealed an additional band of higher molecular weight corresponding to the Fab-peptide adduct. This band resulted from the formation of a covalent bond between the *p*BPA moiety and the peptide. We did not identify which residue (or residues) of the peptide that reacted with *p*BPA because of the unspecific nature of the cross-linking reaction [21]. In contrast, the band corresponding to the covalent adduct was absent when *p*BPA was introduced in the position of $Trp100_{HC}$ of the Fab (Fig. 3d). Importantly, the same photo-cross-linking pattern, i.e. crosslinking with peptide when the Fab was mutated at position $100b_{HC}$, but not when mutated at position 100_{HC}, was observed when the experiment was performed in the presence of lipid membranes (Fig. 3d). This latter observation suggests that the $Trp100b_{HC}$ of the WT Fab locates in the immediate vicinity of the gp41 peptide in a membrane environment.

Design of non-invasive mutants to study the role of each tryptophan residue.

To determine the functional relevance of the two Trp residues of the apex without mutating them, we modified the length of the CDRH3. With the idea of repositioning $Trp100b_{HC}$ or $Trp100_{HC}$, we constructed two different mutants in which either the N-terminal side or the C-terminal side of the apex of the CDRH3 was shifted by introducing a rigid frame made of two proline residues. These proline residues were inserted between $Gly100c_{HC}$ and $Lys100d_{HC}$, or between $Thr98_{HC}$ and $Gly99_{HC}$, to render the two mutants termed Cpro and Npro, respectively (Fig. 4a). The mutant Npro was designed with the expectation that the position of the proximal $Trp100b_{HC}$ would be little affected, and therefore this residue would remain in close proximity to

the peptide. In contrast, in the Cpro mutant the residue Trp100b$_{HC}$ is expected to shift from the position adopted in WT antibody, thus affecting the distance to the peptide (Fig. 4a).

We first verified that the mutations were not detrimental to the stability of the antibodies (Table 1). Second, we employed X-ray crystallography in an attempt to determine the position of the CDRH3 apex in the Fab-peptide complex. Despite the high-resolution achieved (1.48 Å) the position of the Trp100b$_{HC}$ in Npro could not be confirmed because this region was disordered in the crystal (Fig. 4b and Table 2). Except for this region, the structure of the Fab was essentially indistinguishable to that of WT Fab (rmsd-Cα = 0.13 Å). No crystal structure of Cpro was obtained. Npro and Cpro conserved the same sequence (^{100}WGWL^{100c}), and accordingly both mutants interacted with lipid vesicles to a similar extent (Fig. 4c).

Photo-cross-linking experiments in which Trp100b$_{HC}$ was replaced by *p*BPA, confirmed the proximity of this position of the apex to MPER in the bound state of Npro, but not in that of Cpro (Fig. 4d). The inability of the Cpro variant mutated with *p*BPA to crosslink with the peptide indicated that the position 100b$_{HC}$ is no longer close to the peptide in the bound form (Fig. 4d). On the contrary, the mutant Npro displayed the same photo-cross-linking pattern (Fig. 4d) as that of WT Fab described above (Fig. 3b).

Functional consequences of displacing the tryptophan residues.

The influence of displacing each tryptophan residue by using the mutations described above, Npro and Cpro, on the function of the antibody was evaluated by employing cell entry inhibition assays (Fig. 5 and Table 1). The Npro mutant was almost indistinguishable from the WT in assays based on a sensitive HXB2 strain, while the IC$_{50}$ of the Cpro mutant increased by 20-fold. In the more resistant JRCSF strain, both mutations decreased the potency of the antibody, although Cpro was clearly less potent than Npro by *c.a.* 3-fold. Thus, despite having

similar capacity to interact with membranes, the displacement of $Trp100b_{HC}$ from its native position in the mutant Cpro resulted in weaker biological activity in comparison with that of Npro, in which the affected residue was $Trp100_{HC}$.

To determine if the changes in the biological function were caused by a defective ability to engage the epitope in solution, we determined the dissociation constant (K_D) by the high-resolution technique of isothermal titration calorimetry. The titration of WT, Npro and Cpro antibodies with MPER(664-690) in the presence of DPC did not reveal significant differences among the three antibodies. The K_D values were 4.6, 6.2, and 6.9 nM for WT, Npro and Cpro, respectively (Fig. 6a-c and Table 1). Moreover, the relative contribution of two key thermodynamic parameters, such as enthalpy and entropy to the binding free energy of the peptide to the antibody, was very similar to each other (Table 1). We thus conclude that the mutations did not affect the recognition of the epitope in solution. This conclusion is consistent with previous research, in which ablation of the apex did not appreciable change the affinity for the epitope in solution [11].

Since the natural epitope is located on the membrane, we next investigated the impact of these mutations (Npro and Cpro) on the binding ability when the epitope is presented in an environment that better mimics the viral membrane (Fig. 6d,e). To that purpose, and prior to each assay, the MPER(671-693) was fully anchored to the liposomes following the reported methodology [14]. The binding of the Fab to vesicles decorated with MPER was estimated from the relative abundance of antibody co-localized with the vesicles (fraction 4) in a flotation assay. Efficient binding of the Fab to the peptide inserted into the membrane was achieved with WT 4E10 and with Npro Fab, as demonstrated by the high abundance of these two antibodies in the fractions co-floating with the liposomes. In contrast, a significant fraction of the Cpro mutant was observed in the dense fractions suggesting a defect in binding of this mutant to the membrane-

inserted peptide (Fig. 6d). Under these experimental conditions the position $100b_{HC}$ of the *p*BPA-Npro mutant remains in close proximity to the peptide in a lipid membrane similarly to the WT 4E10 Fab. This conclusion is deduced from the additional band observed in the SDS-PAGE, corresponding to the cross-linked adduct of the sample containing *p*BPA-Npro incubated with the vesicles decorated with the epitope (Fig. 6e).

These results suggest that the assay carried out in solution did not capture all the complexity of the binding events that must occur in the environment of the viral membrane. Moreover, we have demonstrated that the $Trp100b_{HC}$ in close proximity to the MPER/TMD region is not only critical for the neutralization potency of the antibody, but also for epitope binding in a membrane context.

DISCUSSION

Broadly neutralizing anti-HIV-1 antibodies against the MPER region of gp41 are at the forefront of novel vaccination strategies to counter the devastating effects of AIDS. These antibodies have the extraordinary ability to recognize the helical MPER epitope at the viral membrane interface. To achieve their function, anti-MPER bNAbs have acquired long CDRH3 loops characterized by a very hydrophobic tip that we term apex. Indeed, mutational studies demonstrate that the hydrophobic and aromatic residues of the apex of the CDRH3 of these bNAbs are essential for viral neutralization [4-6,13,15]. Specifically, in the bNAb 4E10, tryptophan residues at positions 100_{HC} and $100b_{HC}$ are strictly required for biological activity. Despite their overall importance, the location of those residues when the antibody binds MPER in a membrane context was unknown. In this regard, knowledge on the neutralization-competent structure adopted by the CDRH3 apex could help elucidate the recognition mechanism at

interfaces of this singular class of antibody, helping to shape novel vaccination strategies to deter infections by HIV-1.

Here we have showed that viral inhibition by 4E10 is dependent on a minimum of hydrophobicity at the CDRH3 that is correlated with the propensity of the antibody to bind to lipid membranes. However, we have observed important specific effects at the residue level, particularly at the position of the two key tryptophan residues $Trp100_{HC}$ and $Trp100b_{HC}$. Shuffling the residues of the apex region of the CDRH3, while keeping a constant hydrophobicity, or even increasing the hydrophobicity by the incorporation of an additional Trp residue, only resulted in weaker neutralization potency. These observations suggest a more complex role of the CDRH3 region in neutralization, beyond a mere role in membrane attachment.

Comparison of the crystal structures of the 4E10 antibody in the unbound and the bound forms reveals a strong reduction of the B-factors of the regions encompassing CDRH1, CDRH2, and CDRL3 upon peptide binding [11]. However, the residues at the apex $Trp100_{HC}$–$Leu100c_{HC}$ remained highly dynamic suggesting their predisposition to establish further interactions, for example, in the context of the viral membrane. Because the CDRH3 apex projects away from the bound helical peptide, the establishment of interactions with the epitope would imply the reorientation of that portion of the loop. In agreement with this idea, we have formally shown that both Trp residues of the CDRH3 apex insert into the lipid membrane (Fig. 2). In this context, we propose that the free energy of adherence and insertion into the membrane interface, bestowed by these two Trp residues, represents an important driving force for the structural reorientation of the CDRH3 loop towards the lipid, as inferred from the recent crystallographic structure of 4E10 co-crystallized with the lipid PA (6:0) [10]. A possible downside of this mechanism for vaccine design could be the potential development of polyreactivity in the resulting anti-MPER antibody.

We have also demonstrated that the Trp residues at the apex of the CDRH3 play a prominent role beyond favoring the interaction with the membrane. By incorporating a genetically encoded photoreactive residue, we have demonstrated that the position $100b_{HC}$ of 4E10 is contacting MPER/TMD, suggesting that interactions between $Trp100b_{HC}$ and the epitope are critical for the neutralization potency of the antibody (Figs. 3-5). In contrast, a close distance between position 100_{HC} and the peptide was not detected in the photo-cross-linking assays using an analogous approach. This difference suggests that both Trp residues do not contribute following the same pattern to the biological function of the antibody. The data indicate that $Trp100_{HC}$ must contribute to the overall activity of the antibody by stabilizing the antibody-peptide complex in a more indirect manner. In contrast, specific interactions involving $Trp100b_{HC}$ with this region of gp41 might occur in a manner analogous to that of the 10E8 antibody [14].

The biological relevance of the position of the $Trp100b_{HC}$ to mediate additional interactions with the TMD was revealed by employing an engineered mutant where the position of $Trp100b_{HC}$ was shifted. The displacement of $Trp100b_{HC}$ had a deleterious effect on the ability of the antibody to interact with the MPER/TMD region, neutralize PsVs, and efficiently engage the epitope when embedded in the membrane. However, the affinity constant (K_D) of 4E10 for MPER peptide in solution was unaltered. These contrasting observations clearly indicate that binding in solution does not capture the complex process of neutralization occurring at the constrained environment of the viral membrane.

The data presented herein suggest that in the presence of a lipid membrane, $Trp100b_{HC}$–MPER/TMD interactions are stabilized by the surrounding lipids, perhaps by decreasing the dissociation rate constant (k_{off}) of the peptide-lipid-antibody complex. This is a matter of great interest that will need to be resolved in the immediate future. It is also likely that full stabilization

of such complex requires the presence of $Trp100_{HC}$. Interaction of $Trp100_{HC}$ with surrounding lipids as previously suggested [10], together with the simultaneous interaction of the $Trp100b_{HC}$ reported here with the TMD (see the model in Fig. 7) could represent the neutralization-competent conformation adopted by the apex of the CDRH3. The interaction of 4E10 with residues embedded in the membrane, such as Lys/Arg-683, is supported by the recent NMR structure of the TMD trimer (residues 677-716) in bicelles [22]. However, lack of critical residues belonging to the epitope of MPER in this structure, which are necessary for the recognition by 4E10, limits a more in depth analysis. We speculate that the resulting gp41-antibody-lipid complex involving both CDRH3 Trp residues would efficiently zip the contact surface between the antibody and gp41 interrupting MPER conformational changes during the fusion process and, ultimately, preventing viral infection.

In summary, we report the dual role of the two Trp residues of the apex of the CDRH3 of 4E10, and specially that of $Trp100b_{HC}$, for the recognition of gp41 at the membrane interface, and for its neutralization potency. This work contributes to (i) clarify the molecular basis by which the 4E10 antibody exerts effective neutralization, and (ii) to guide future formulations to design and to develop an efficient vaccine against HIV infection based on anti-MPER antibodies.

MATERIALS AND METHODS

Materials.

The peptides were synthesized in the C-terminal carboxamide form by solid-phase methods using Fmoc chemistry, purified by reverse phase high-pressure liquid chromatography, and characterized by matrix-assisted time-of-flight mass spectrometry (purity >95%). Peptides were routinely dissolved in DMSO (except for the ITC experiments, see below) and their concentration determined by the bicinchoninic acid microassay (Pierce, Rockford, IL, USA) or

by their absorbance at 280 nm (for ITC experiments). The final concentration of peptide was adjusted in assay buffer, resulting in a concentration of DMSO of 0.5 % or less in all cases. Goat anti-human IgG-Fab antibody was purchased from Sigma (St. Louis, MO). Secondary antibody conjugated to horseradish peroxidase (HRP), mouse anti-goat IgG-HRP and rabbit anti-human IgG-HRP was purchased from Santa Cruz (Heidelberg, Germany). Vector pEVOL, encoding a tRNA synthetase suitable for the incorporation of the photoreactive amino acid, *p*BPA, was a gift from Prof. P. G. Schultz (The Scripps Research Institute, CA) [23]. The compound *p*BPA was purchased from Bachem (Bubendorf, Switzerland). The fluorescent probe NBD was from Thermofisher (Eugene, Oregon). Lipids 1,2-dioleoyl-*sn*-glycero-3-phosphocholine (DOPC), 1,2-dioleoyl-*sn*-glycero-3-phosphoethanolamine (DOPE), 1,2-dioleoyl-*sn*-glycero-3-phosphoserine (DOPS), sphingomyelin (SM), cholesterol (Chol), 1-palmitoyl-2-oleoyl-*sn*-glycero-3-phosphocholine (POPC), and 1,2-dioleoyl-*sn*-glycerol-3-phosphoethanolamine-N-(lissamine rhodamine B sulfonyl) (Rho-PE) were purchased from Avanti Polar Lipids (Alabaster, Alabama).

Production and characterization of Fabs.

The sequences of 4E10 were cloned in the plasmid pColaDuet and expressed in *Escherichia coli* T7-shuffle strain. Recombinant expression was induced at 18 °C overnight with 0.4 mM isopropyl-D-thiogalactopyranoside when the culture reached an optical density of 0.8. Cells were harvested and centrifuged at 8,000 × *g*, after which they were resuspended in a buffer containing 50 mM HEPES (pH 7.5), 500 mM NaCl, 35 mM imidazole, DNase (Sigma-Aldrich, St. Louis, MO) and an EDTA-free protease inhibitor mixture (Roche, Madrid, Spain). Cell lysis was performed using an Avestin Emulsiflex C5 homogenizer. Cell debris was removed by centrifugation, and the supernatant loaded onto a nickel-nitrilotriacetic acid (Ni-NTA) affinity column (GE Healthcare). Elution was performed with 500 mM imidazole, and the fractions containing the His-tagged proteins were pooled, concentrated and dialyzed against 50 mM

sodium phosphate (pH 8.0), 300 mM NaCl, 1 mM DTT, and 0.3 mM EDTA in the presence of purified protease Tobacco etch virus [24]. Fabs were separated from the cleaved peptides containing the His_6 tag by an additional step in a Ni-nitrilotriacetic column. The flow-through fraction containing the antibody was dialyzed overnight at 4 ºC against sodium acetate (pH 5.6) supplemented with 10% glycerol and subsequently loaded onto a MonoS ion exchange chromatography column (GE Healthcare). Elution was carried out with a gradient of potassium chloride and the fractions containing the purified Fab concentrated and dialyzed against a buffer containing 10 mM sodium phosphate (pH 7.5), 120 mM NaCl, and 10% glycerol. For the preparation of 4E10 mutants, the KOD-Plus mutagenesis kit (Toyobo, Osaka, Japan) was employed following the instructions of the manufacturer.

Membrane partition assays.

The partition of the antibody into membranes was examined by vesicle flotation experiments in sucrose gradients following the method described by Yethon *et al* [25]. In brief, 100 µl of large unilamellar vesicles (LUVs) of various compositions and labeled with the lipid rhodamine-PE (Avanti Polar lipids, Alabaster, AL), were adjusted to a sucrose concentration of 1.4 M in a final volume of 300 µl, and subsequently deposited of a stepwise gradient composed of successive solutions containing 0.8 M (400 µl) and 0.5 M sucrose (300 µl). The gradient was centrifuged at 436,000 × *g* for 3 h in a TLA120.2 rotor (Beckman Coulter, Brea, CA). After centrifugation, four fractions each of 250 µl were collected. The material adhered to the centrifugation tubes was obtained by washing the tubes with 250 µl of a solution of 1% (w/v) SDS at 100 °C. The VL vesicles were composed by the lipids DOPC, Chol, SM, DOPE and DOPS in a molar ratio of 14:46:17:16:7 [26].

Inhibition of cell entry.

For the assays of the inhibition of cell infection [15,27], HIV-1 PsVs were produced by transfection of human kidney HEK293T cells with the full-length env clone JRCSF or PIIIenv (kindly provided by Dr. Jamie K. Scott and Dr. Naveed Gulzar, Simon Fraser University, BC, Canada) using calcium phosphate. Cells were co-transfected with vectors pWXLP-GFP and pCMV8.91, encoding a GFP and an env-deficient HIV-1 genome, respectively (provided by Patricia Villace, CSIC, Madrid). After 24 h, the medium was replaced with Optimem-Glutamax II (Invitrogen, Paisley, UK) without serum. Three days after transfection, the PsVs were harvested, passed through sterile filters of 0.45 μm pore-size (Millex® HV, Millipore NV, Brussels, Belgium), and finally concentrated by ultracentrifugation in a sucrose gradient. Neutralization was determined using TZM-bl target cells (AIDS Research and Reference Reagent Program, Division of AIDS, NIAID, NIH, contributed by J. Kappes). Samples were set up in duplicate in 96-well plates, and incubated for 1.5 h at 37 °C with a 10-15% tissue culture infectious dose of PsVs. After co-incubation of antibody with PsVs, 11,000 target cells were added in the presence of 30 μg/mL DEAE-dextran (Sigma-Aldrich, St. Louis, MO). Neutralization levels after 72 h were inferred from the reduction in the number of GFP-positive cells as determined by flow cytometry using a BD FACSCalibur Flow Cytometer (Becton Dickinson Immunocytometry Systems, Mountain View, CA).

Penetration of NBD-labeled Fab in membranes.

Fabs were labeled with a polarity-sensitive probe as described earlier [28,29]. Succinctly, a Fab mutated with a cysteine residue at the desired position ($Trp100_{HC}Cys$ or $Trp100b_{HC}Cys$) was generated by site-directed mutagenesis, and then modified with the sulfhydryl-specific iodoacetamide derivative NBD to yield the corresponding labeled Fab. Fluorescence-emission spectra were recorded with the excitation wavelength fixed at 470 nm. The emission spectrum of a sample of unlabeled antibody was subtracted from the spectrum of the corresponding sample

containing the labeled Fab obtained under the same experimental conditions. Fluorescence spectra of NBD were obtained upon incubation of NBD-labeled Fab (0.15 μM) with increasing concentrations (25, 50, 100, 150 and 250 μM) of vesicles composed of lipids (DOPC:DOPE:DOPS:SM:Chol) (14:16:7:16:47 molar ratio) mimicking the viral membrane (VL-like), or with proteoliposomes lacking Chol and composed of (DOPC:DOPE:DOPS:SM) (27:29:14:30 molar ratio) at a fixed concentration of lipid (250 μM) containing increasing concentrations of the peptide MPER(671-693) (0.25, 0.5, 1.0, 1.7, 3.4, and 6.8 μM). Chol was not included in the vesicles decorated with peptide to avoid interference with the measurements by aggregation of vesicles observed with high peptide loads [30].

Photo-cross-linking assay with a genetically encoded unnatural amino acid.

For the photo-cross-linking experiments an amber codon specific for an engineered tRNA that translates the unnatural amino acid *p*BPA was encoded in the DNA sequence of the heavy chain of the 4E10 Fab. Procedures to express the 4E10 Fab mutein bearing *p*BPA instead of Trp at position 100_{HC} or at position $100b_{HC}$ were adapted from previous reports [23,31]. Synthesis of Fab and the engineered tRNA was induced with 0.4 mM IPTG and 4% (w/v) arabinose, respectively, in LB medium supplemented with 0.2 mg/L of *p*BPA. For the photo-cross-linking experiment, mixtures containing Fab bearing the *p*BPA substitution at 1.5 μM and peptides at 10 μM were incubated and irradiated with UV-light at 365 nm for 20 min at 4 °C using a UVP B-100AP lamp. Peptide was presented to the antibody in aqueous solution in micelles of DPC (5 mM), or inserted into membranes of POPC:Chol (1:1 molar ratio, 1.5 mM). The heavy chain of Fab-peptide adducts were separated by SDS-PAGE and stained with Coomassie blue. Photo-cross-linked products were monitored using an LAS-4000 image analyzer (GE Healthcare).

Differential scanning calorimetry.

The thermal stability of Fabs was inferred by the technique of differential scanning calorimetry using a VP-DSC system (MicroCal, Northampton, MA). All thermal scans were performed in a buffer composed of 10 mM monosodium phosphate (pH 7.5), 150 mM NaCl, and 10% glycerol. Protein samples at 10 μM were heated from 30 to 90 ºC at a constant rate of 1 ºC min^{-1}. The ORIGIN software package (MicroCal) was used for data collection and analysis. The buffer baseline was subtracted from the raw data, which was subsequently normalized by protein concentration and a non-two-state model was fitted to the data to obtain the thermodynamic parameters displayed in Table 1.

Isothermal titration calorimetry.

Calorimetric titration experiments were performed with a VP-ITC microcalorimeter (MicroCal, Northampton, MA) at 25 ^{o}C. Prior to the experiment, proteins were dialyzed o/n at 4 ºC against 10 mM sodium phosphate (pH 7.5), 150 mM NaCl, and 10% glycerol, and degassed just before the measurement. The Fab 4E10 WT (3 μM) in dialysis buffer supplemented with 5 mM DPC was titrated with 40 μM of peptide (dissolved and prepared in dialysis buffer supplemented with 5 mM DPC but without DMSO). The volume of each injection was 10 μL. Peptide dilution heat was subtracted from the experimental and final data. The binding isotherms were fitted to a one-site binding model using the program ORIGIN 7.0. The fitting yields the stoichiometry (n), the binding constant (K_D) and the enthalpy ($\Delta H°$) of the binding reaction (Table 1).

Crystallization of 4E10 Fab-peptide complex, data collection and structure refinement.

Crystals of the complex between Npro Fab (3 mg/ml) and the peptide MPER(671-683) prepared by incubating antibody and peptide at a molar ratio of ~1:1.3 were grown in a solution of 100 mM sodium acetate (pH 5.0), 34% PEG 4000, and 225 mM ammonium acetate at 18 °C. A single protein crystal was harvested, cryoprotected by immersion in crystallization solution

supplemented with 10% glycerol, and stored in liquid nitrogen until data collection at the synchrotron. Diffraction data from a single crystal were collected on beamline BL13-XALOC of the ALBA Cell Synchrotron (Barcelona, Spain) under cryogenic conditions (100 K). Diffraction images were processed with the program MOSFLM and merged and scaled with the program SCALA of the CCP4 suite [32]. The three-dimensional structure was determined by molecular replacement using the coordinates of 4E10 (PDB entry code 4WY7) [6] with the program PHASER [33]. The initial model was further refined with the programs REFMAC5 [34] and COOT [35]. Validation was carried out with PROCHECK [36]. Data collection and refinement statistics are summarized in Table 2.

Accession Numbers

The coordinates and structure factors of Npro in complex the peptide MPER(671-683) have been deposited in the PDB under entry code 5X08.

Acknowledgements

We thank Dr. Morante (The University of Tokyo), Dr. Kudo (The University of Tokyo), and Dr. Apellaniz (UPV/EHU) for valuable discussions and technical advice. This work was supported by a JSPS KAKENHI-C grant 15K06962 (to J.M.M.C.), the NIH and the Basque Government (grants AI097051 and IT838-13 to J.L.N.), the Platform for Drug Discovery, Informatics and Structural Life Science from the Ministry of Ministry of Education, Culture, Sports, Science and Technology of Japan (to K.T.) and by JSPS KAKENHI-A grants 25249115 and 16H02420 (to K.T.). E.R. was recipient of a predoctoral fellowship from the Basque Government.

Competing financial interests

The authors declare no competing financial interests.

Author contributions.

E.R., K.T, J.L.N., and J.M.M.C. conceived the research and designed the experiments; E.R. produced Fabs, performed biophysical and biochemical characterizations with assistance of S.I. and M.G.-M; E.R. and J.M.M.C. obtained crystals with assistance of R.S.; J.M.M.C. determined and refined the X-ray crystal structure; E.R. and R.S. produced the molecular model for recognition in membranes; E.R., J.L.N., and J.M.M.C. wrote the paper; all authors approved the manuscript.

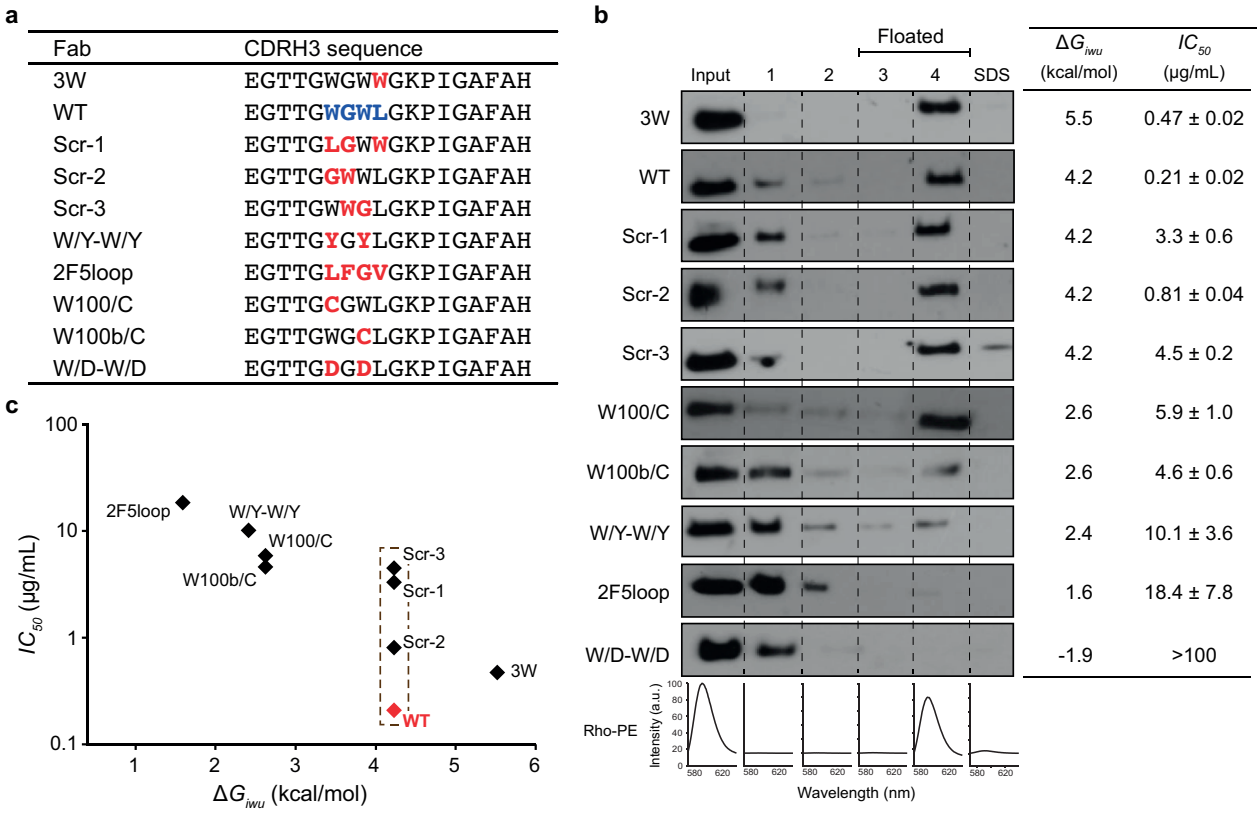

Figure 1. Multivariate mutagenesis analysis of the apex loop of CDRH3. (a) List of sequences of CDRH3 examined. The mutated residues of the apex of the CDRH3 loop (defined as residues ^{100}WGWL^{100c}) are indicated in red. The two key tryptophan residues present in the apex are located at positions 100_{HC} and $100b_{HC}$. **(b)** For each variant of Fab three properties were analyzed: Binding of Fab to VL vesicles by the flotation method (left), hydrophobicity-at-interface [18] (center), and neutralization potency against HXB2 PsVs (right). The co-localization of vesicles and Fab was demonstrated by comparing the position of the protein as shown by western-blot, with the fluorescence signal of the lipid Rho-PE (bottom). Lanes 1-4 of the western-blot correspond to samples of each of the four 250-μl fractions collected from the centrifugation tube, from bottom to top. The material adhered to the tubes was collected into a fifth fraction (labeled SDS). **(c)** The hydrophobicity-at-interface for each variant of Fab is plotted versus its viral neutralization potency. The mutant W/D-W/D does not display a measurable neutralization and therefore was not included in this plot. The hydrophobicicty of the constructs enclosed in the dashed line box is constant, but their inhibitory potency varies significantly.

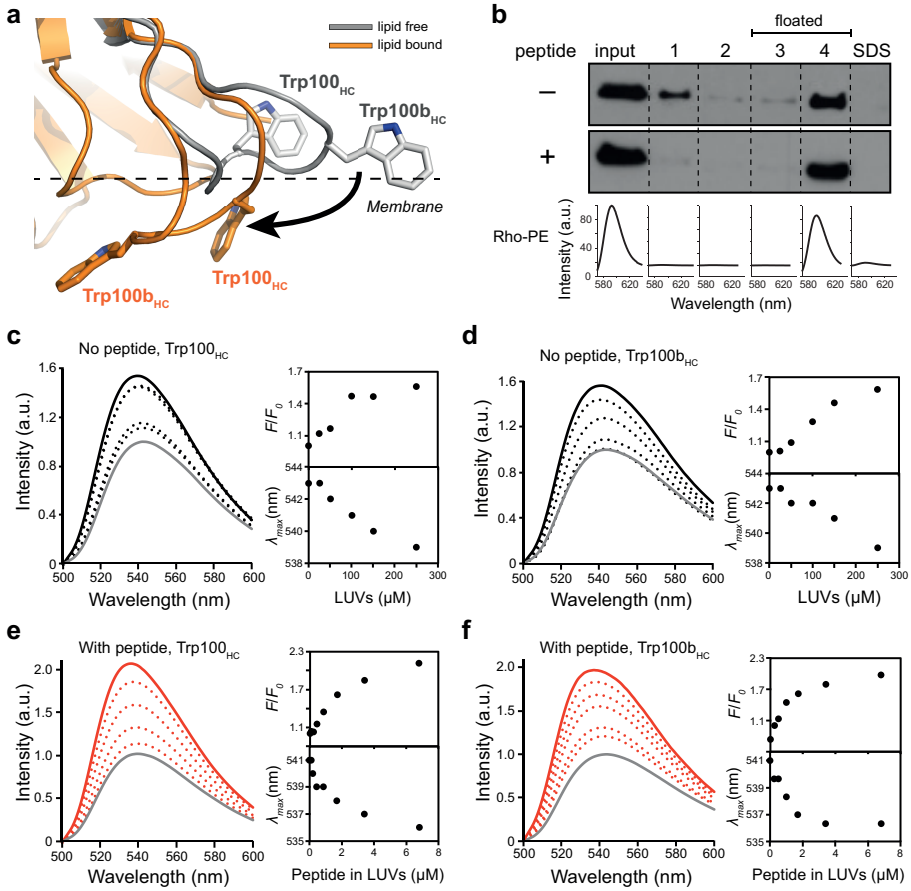

Figure 2. Insertion of the apex of CDRH3 into membranes. (a) Cartoon representation of the conformational change of CDRH3 triggered by the interaction with the membrane, as suggested by Irimia et al. [10]. The coordinates of 4E10 Fab in complex with MPER(671-683) (gray, PDB entry code 2FX7) and in complex with the lipid PA (6:0) (orange, PDB entry code 4XBG) were superimposed. Residues $Trp100_{HC}$ and $Trp100b_{HC}$ are shown in stick representation and the approximate position of the outer surface of the membrane indicated by the dotted line (inferred from the position of bound lipids, not shown). **(b)** Partitioning of 4E10 Fab into membranes in the absence (top) and presence (middle) of peptide MPER(671-693) as estimated by the flotation method. **(c-f)** Fluorescence emission spectra of Fab-s labeled with the dye NBD. Emission spectra of Fab labeled with NBD at positions 100_{HC} **(c)** or $100b_{HC}$ **(d)** were measured in solution (gray solid line) or in the presence of increasing concentrations of VL vesicles (black solid and dotted lines). Analogous experiments with the Fab labeled at position 100_{HC} **(e)** or position $100b_{HC}$ **(f)** were performed with VL vesicles w/o Chol and decorated with MPER(671-693) (red solid and dotted lines). Each set of spectra is complemented with plots showing the changes in fluorescence intensity, and the position of the maximum of fluorescence emission (λ_{max}). The initial value of fluorescence (F_0) was determined from the maximum intensity of the labeled Fab in solution (panels c and d, gray traces), or from labeled Fab in the presence of liposomes devoid of cholesterol and w/o peptide (panels e and f, gray traces). LUV refer to large unilamellar vesicles.

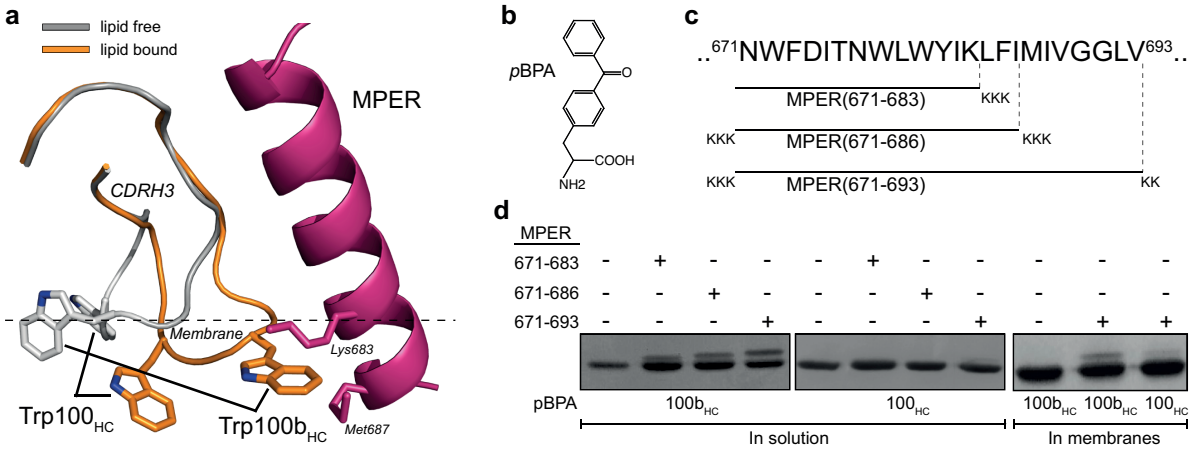

Figure 3. Proximity between CDRH3 of 4E10 and MPER in solution and in membranes. (a) Model of the conformational change of CDRH3. This model is based on the comparison between the crystal structure of Fab in complex with MPER(671-683) (gray loop, PDB entry code 2FX7) and that of unbound Fab in the presence of lipid PA (6:0) (orange loop PDB entry code 4XBG). To give a more complete view of MPER, the structure of the longer peptide MPER(664-690) (PDB entry code 5GHW) obtained after superimposition on the shorter MPER(671-683) (PDB entry code 2FX7) is shown. **(b)** Structure of the genetically encoded amino acid *p*BPA. **(c)** Sequence of the three MPER peptides employed. Three peptides that included different extents of the TMD were evaluated. **(d)** Photo-cross-linking between 4E10 Fab labeled with the genetically encoded probe *p*BPA at position 100_{HC} or $100b_{HC}$, and the three MPER peptides indicated in the panel above. The experiment was carried out in the presence of the detergent DPC (in solution), or in the presence of vesicles composed of the lipids POPC:Chol (1:1). SDS-PAGE was performed under reducing conditions, resulting on an apparent single band corresponding to the heavy and light chains.

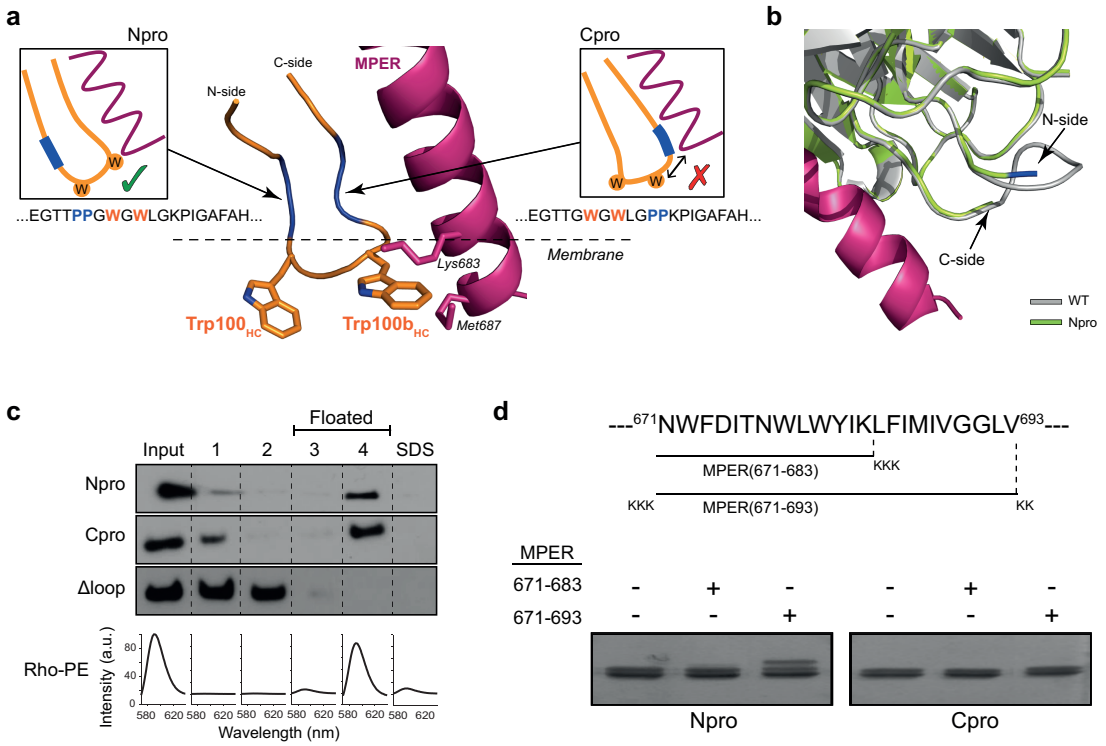

Figure 4. The length of the CDRH3 governs the membrane properties of 4E10. (a) Schematic representation of the two strategies to elongate the CDRH3 region employed herein. The variant Npro was prepared by introducing two proline residues (a rigid scaffold) between residues Thr98$_{HC}$ and Gly99$_{HC}$ on the N-side of the CDRH3 (in blue, left side). Cpro was generated by introducing two proline residues between Gly100c$_{HC}$ and Lys100d$_{HC}$ on the C-side of CDRH3 (depicted in blue, right side), resulting in the presumable displacement of Trp100b$_{HC}$ away from the peptide with respect to WT Fab. The shorter Δloop construct lacking the two tryptophan residues of the CDRH3 is described in a previous study [6]. **(b)** Superposition of the crystal structure of WT 4E10 (gray) (PDB entry code 2FX7) and Npro (green, this study). Both structures were obtained in complex with MPER(671-683) (dark pink). Because of dynamic disorder, only one of the proline residues introduced in the mutant was modelled in the crystal structure. The position of other residues of the apex (PGWGWL) could not be modelled. **(c)** Partitioning of Npro and Cpro into VL vesicles using the same methodology described in Figure 1. The construct ΔLoop in which the CDRH3 apex had been ablated was employed as a negative control [6]. **(d)** Photo-cross-linking experiment of Npro and Cpro mutants, each modified with *p*BPA at position 100b$_{HC}$, with short and long versions of MPER in aqueous solution in the presence of the detergent DPC.

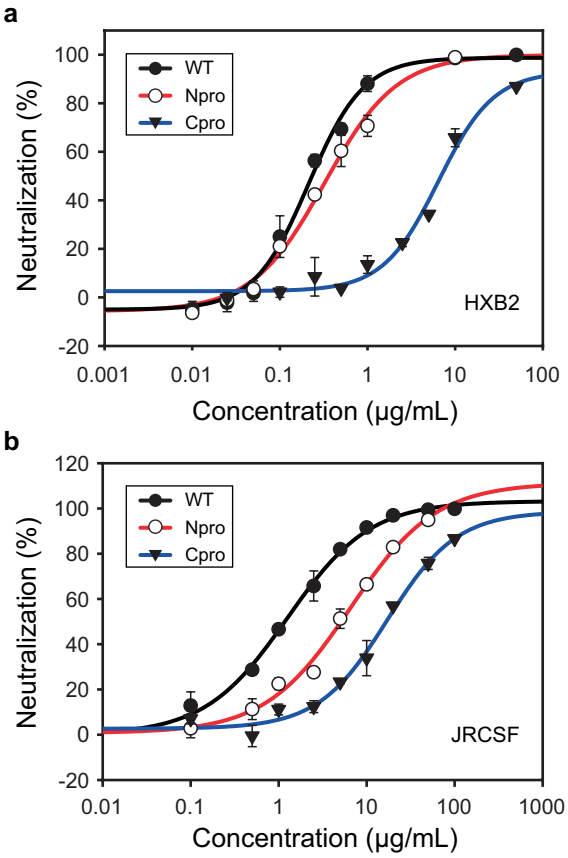

Figure 5. Neutralization potency of Npro and Cpro. The potency of WT 4E10 (filled circles, black line), as well as the two elongated versions of 4E10, Npro (empty circles, red line) and Cpro (filled triangles, blue line), was evaluated in a cell entry inhibition assay against **(a)** PsVs HXB2 and **(b)** PsVs JRCSF.

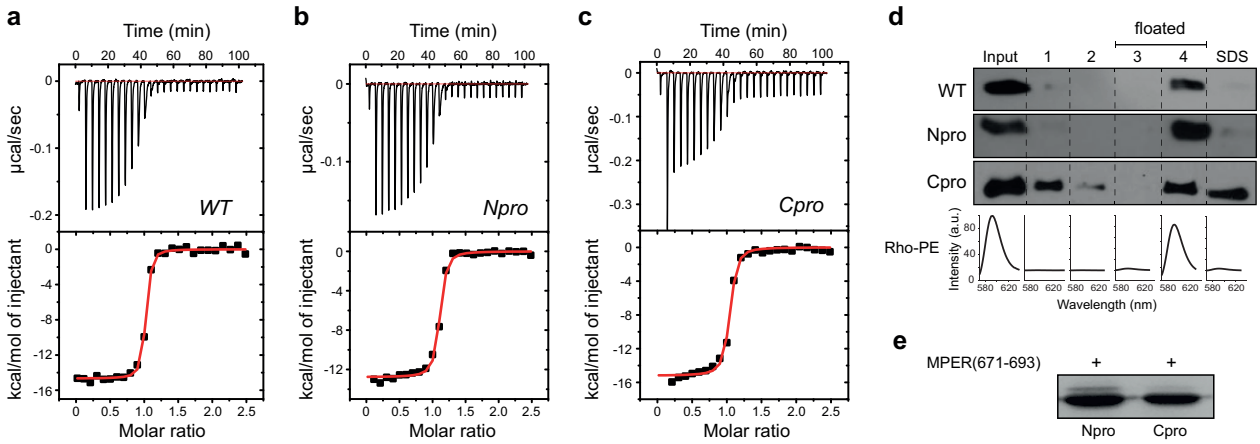

Figure 6. Recognition mode of the epitope in solution and in membranes. Binding isotherm of MPER(664-690) to **(a)** 4E10 WT, **(b)** Npro, and **(c)** Cpro in the presence of DPC. **(d)** Recognition of the MPER epitope in the presence of lipid membranes. The flotation experiment was carried out to evaluate the binding of 4E10 WT or the elongated mutants (Npro or Cpro) to membranes decorated with the epitope MPER(671-693). The lipid composition of the vesicles was POPC:Chol (1:1) to minimize the spontaneous binding (peptide independent) of the antibody to the membranes. **(e)** Photo-cross-linking assay of Npro and Cpro versions of 4E10, modified with *p*BPA at position $100b_{HC}$, with MPER(671-693) inserted into membranes of POPC:Chol (1:1).

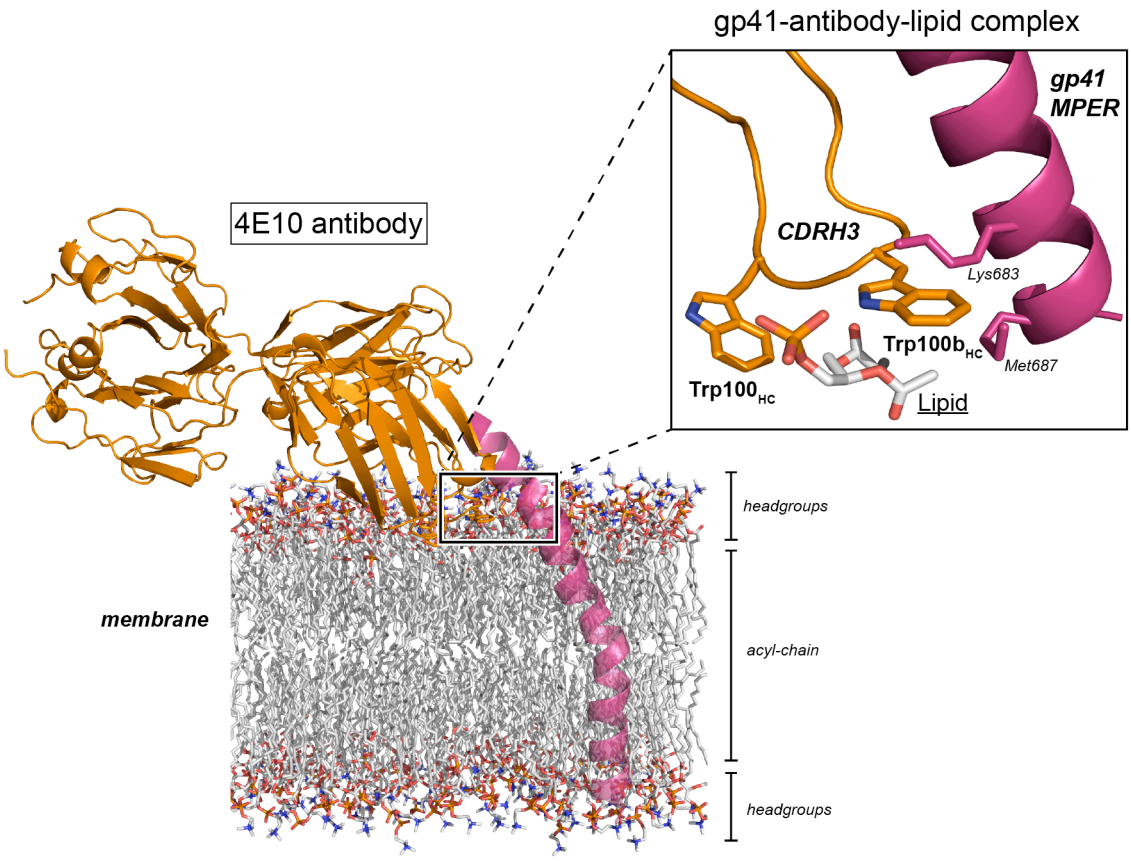

Figure 7. Model of recognition of the MPER epitope by 4E10 in membranes. 4E10 antibody is shown in orange, the MPER/TMD region in dark pink (50% transparency) and lipid molecules in gray (carbon), blue (nitrogen), red (oxygen) and dark orange (phosphate). Inset: close-up view of the gp41-4E10 antibody-lipid complex showing the proximity of Trp100b$_{HC}$ to residues of the TMD. A lipid molecule located between the Trp residues of the CDRH3 may facilitate the stability of the complex between antibody and peptide at the membrane interface. This model was based on PDB entry codes 4XBG [10] and 5GHW [14]. The model of the phospholipid bilayer was constructed from a model containing 200 molecules of POPC.

Table 1. Thermal stability, neutralization potency and binding of peptide MPER(664-690).

4E10	T_M (ºC)	ΔT_M (ºC)	HXB2 IC_{50} (µg/mL)	JRCSF IC_{50} (µg/mL)	K_D (nM)	$\Delta H°$ (kcal mol^{-1})	$-T\Delta S°$ (kcal mol^{-1})[a]	n[b]
WT	69.8	n.a.	0.21 ± 0.02	1.3±0.1	4.6 ± 1.5	−15.1 ± 0.2	3.7	1.0 ± 0.1
Npro	68.6	1.1	0.30 ± 0.08	6.5 ± 1.6	6.2 ± 1.3	−12.8 ± 0.1	1.6	1.1 ± 0.1
Cpro	67.5	2.3	6.4 ± 1.4	17 ± 4	6.9 ± 1.5	−15.2 ± 0.2	4.0	1.0 ± 0.1

[a] Temperature was 25 °C.
[b] n refers to the molar ratio of peptide to antibody.

Table 2. Data collection and refinement statistics.[a]

	4E10 Npro + peptide
Data collection	
Space group	C2
Cell dimensions	
a, *b*, *c* (Å)	157.5, 44.5, 85.1
α, *β*, *γ* (°)	90.0, 113.7, 90.0
Resolution (Å)	22.3 – 1.49 (1.57 – 1.49)
No. unique reflections	88,101 (12,788)
R_{merge} (%)	8.1 (70.7)
R_{pim} (%)	3.5 (34.4)
$I / \sigma I$	11.9 (2.4)
$CC_{1/2}$	0.998 (0.666)
Completeness (%)	99.5 (99.5)
Redundancy	6.0 (5.8)
Refinement	
Resolution (Å)	22.3 – 1.49
No. reflections	88,093
R_{work} / R_{free}	17.6 / 20.3
No. atoms	
Protein	3,328
Peptide	138
Ligand/ion	13
Water	329
B-factors	
Protein	17.4
Peptide	25.2
Ligand/ion	22.5
Water	25.7
R.m.s. deviations	
Bond lengths (Å)	0.013
Bond angles (°)	1.5

[a]Values in parentheses correspond to the highest-resolution shell.

REFERENCES

[1] J.M. Binley, T. Wrin, B. Korber, M.B. Zwick, M. Wang, C. Chappey, G. Stiegler, R. Kunert, S. Zolla-Pazner, H. Katinger, C.J. Petropoulos, D.R. Burton. Comprehensive cross-clade neutralization analysis of a panel of anti-human immunodeficiency virus type 1 monoclonal antibodies. J. Virol. 78 (2004) 13232-52, 10.1128/JVI.78.23.13232-13252.2004.

[2] P.D. Kwong, J.R. Mascola. Human antibodies that neutralize HIV-1: identification, structures, and B cell ontogenies. Immunity 37 (2012) 412-25, 10.1016/j.immuni.2012.08.012.

[3] D.R. Burton, L. Hangartner. Broadly neutralizing antibodies to HIV and their role in vaccine design. Annu. Rev. Immunol. 34 (2016) 635-59, 10.1146/annurev-immunol-041015-055515.

[4] E.M. Scherer, D.P. Leaman, M.B. Zwick, A.J. McMichael, D.R. Burton. Aromatic residues at the edge of the antibody combining site facilitate viral glycoprotein recognition through membrane interactions. Proc. Natl. Acad. Sci. USA 107 (2010) 1529-34, 10.1073/pnas.0909680107.

[5] S.M. Alam, M. Morelli, S.M. Dennison, H.X. Liao, R. Zhang, S.M. Xia, S. Rits-Volloch, L. Sun, S.C. Harrison, B.F. Haynes, B. Chen. Role of HIV membrane in neutralization by two broadly neutralizing antibodies. Proc. Natl. Acad. Sci. USA 106 (2009) 20234-9, 10.1073/pnas.0908713106.

[6] B. Apellaniz, E. Rujas, S. Serrano, K. Morante, K. Tsumoto, J.M. Caaveiro, M.A. Jimenez, J.L. Nieva. The atomic structure of the HIV-1 gp41 transmembrane domain and its connection to the immunogenic membrane-proximal external region. J. Biol. Chem. 290 (2015) 12999-3015, 10.1074/jbc.M115.644351.

[7] G.H. Bird, A. Irimia, G. Ofek, P.D. Kwong, I.A. Wilson, L.D. Walensky. Stapled HIV-1 peptides recapitulate antigenic structures and engage broadly neutralizing antibodies. Nat. Struct. Mol. Biol. 21 (2014) 1058-67, 10.1038/nsmb.2922.

[8] R.M. Cardoso, F.M. Brunel, S. Ferguson, M. Zwick, D.R. Burton, P.E. Dawson, I.A. Wilson. Structural basis of enhanced binding of extended and helically constrained peptide epitopes of the broadly neutralizing HIV-1 antibody 4E10. J. Mol. Biol. 365 (2007) 1533-44, 10.1016/j.jmb.2006.10.088.

[9] R.M. Cardoso, M.B. Zwick, R.L. Stanfield, R. Kunert, J.M. Binley, H. Katinger, D.R. Burton, I.A. Wilson. Broadly neutralizing anti-HIV antibody 4E10 recognizes a helical conformation of a highly conserved fusion-associated motif in gp41. Immunity 22 (2005) 163-73, 10.1016/j.immuni.2004.12.011.

[10] A. Irimia, A. Sarkar, R.L. Stanfield, I.A. Wilson. Crystallographic identification of lipid as an integral component of the epitope of HIV broadly neutralizing antibody 4E10. Immunity 44 (2016) 21-31, 10.1016/j.immuni.2015.12.001.

[11] E. Rujas, N. Gulzar, K. Morante, K. Tsumoto, J.K. Scott, J.L. Nieva, J.M. Caaveiro. Structural and Thermodynamic Basis of Epitope Binding by Neutralizing and Nonneutralizing Forms of the Anti-HIV-1 Antibody 4E10. J. Virol. 89 (2015) 11975-89, 10.1128/JVI.01793-15.

[12] E. Rujas, N. Gulzar, K. Morante, K. Tsumoto, J.K. Scott, J.L. Nieva, J.M.M. Caaveiro. Reply to "The broadly neutralizing, anti-HIV antibody 4E10: an open and shut case?". J. Virol. 90 (2016) 3276-7, 10.1128/JVI.02970-15.

[13] J. Huang, G. Ofek, L. Laub, M.K. Louder, N.A. Doria-Rose, N.S. Longo, H. Imamichi, R.T. Bailer, B. Chakrabarti, S.K. Sharma, S.M. Alam, T. Wang, Y. Yang, B. Zhang, S.A. Migueles, R. Wyatt,

B.F. Haynes, P.D. Kwong, J.R. Mascola, M. Connors. Broad and potent neutralization of HIV-1 by a gp41-specific human antibody. Nature 491 (2012) 406-12, 10.1038/nature11544.

[14] E. Rujas, J.M.M. Caaveiro, A. Partida-Hanon, N. Gulzar, K. Morante, B. Apellaniz, M. Garcia-Porras, M. Bruix, K. Tsumoto, J.K. Scott, M.A. Jimenez, J.L. Nieva. Structural basis for broad neutralization of HIV-1 through the molecular recognition of 10E8 helical epitope at the membrane interface. Sci. Rep. 6 (2016) 10.1038/Srep38177.

[15] J.P. Julien, N. Huarte, R. Maeso, S.G. Taneva, A. Cunningham, J.L. Nieva, E.F. Pai. Ablation of the complementarity-determining region H3 apex of the anti-HIV-1 broadly neutralizing antibody 2F5 abrogates neutralizing capacity without affecting core epitope binding. J. Virol. 84 (2010) 4136-47, 10.1128/JVI.02357-09.

[16] F. Klein, H. Mouquet, P. Dosenovic, J.F. Scheid, L. Scharf, M.C. Nussenzweig. Antibodies in HIV-1 vaccine development and therapy. Science 341 (2013) 1199-204, 10.1126/science.1241144.

[17] K. Tsumoto, J.M.M. Caaveiro. Antigen-antbody binding. Encyclopedia of Life Sciences (ELS). Chichester: John Wiley & Sons; 2016.

[18] W.C. Wimley, S.H. White. Experimentally determined hydrophobicity scale for proteins at membrane interfaces. Nat. Struct. Biol. 3 (1996) 842-8,

[19] M.G. Gore. Spectrophotometry and spectrofluorimetry: A practical approach. Second ed. New York: Oxford University Press; 2000.

[20] J.R. Lakowicz. Principles of Fluorescence Spectroscopy. New York: Springer; 2007.

[21] G. Dorman, G.D. Prestwich. Benzophenone photophores in biochemistry. Biochemistry 33 (1994) 5661-73, 10.1021/Bi00185a001.

[22] J. Dev, D. Park, Q.S. Fu, J. Chen, H.J. Ha, F. Ghantous, T. Herrmann, W.T. Chang, Z.J. Liu, G. Frey, M.S. Seaman, B. Chen, J.J. Chou. Structural basis for membrane anchoring of HIV-1 envelope spike. Science 353 (2016) 172-5, 10.1126/science.aaf7066.

[23] T.S. Young, I. Ahmad, J.A. Yin, P.G. Schultz. An enhanced system for unnatural amino acid mutagenesis in *E. coli*. J. Mol. Biol. 395 (2010) 361-74, 10.1016/j.jmb.2009.10.030.

[24] T. Kawai, J.M.M. Caaveiro, R. Abe, T. Katagiri, K. Tsumoto. Catalytic activity of MsbA reconstituted in nanodisc particles is modulated by remote interactions with the bilayer. FEBS Lett. 585 (2011) 3533-7, 10.1016/j.febslet.2011.10.015.

[25] J.A. Yethon, R.F. Epand, B. Leber, R.M. Epand, D.W. Andrews. Interaction with a membrane surface triggers a reversible conformational change in Bax normally associated with induction of apoptosis. J. Biol. Chem. 278 (2003) 48935-41, 10.1074/jbc.M306289200.

[26] N. Huarte, P. Carravilla, A. Cruz, M. Lorizate, J.A. Nieto-Garai, H.G. Krausslich, J. Perez-Gil, J. Requejo-Isidro, J.L. Nieva. Functional organization of the HIV lipid envelope. Sci. Rep. 6 (2016) 34190, 10.1038/Srep34190.

[27] S. Serrano, A. Araujo, B. Apellaniz, S. Bryson, P. Carravilla, I. de la Arada, N. Huarte, E. Rujas, E.F. Pai, J.L. Arrondo, C. Domene, M.A. Jimenez, J.L. Nieva. Structure and immunogenicity of a peptide vaccine, including the complete HIV-1 gp41 2F5 epitope: implications for antibody recognition mechanism and immunogen design. J. Biol. Chem. 289 (2014) 6565-80, 10.1074/jbc.M113.527747.

[28] A.P. Heuck, E.M. Hotze, R.K. Tweten, A.E. Johnson. Mechanism of membrane insertion of a multimeric beta-barrel protein: perfringolysin O creates a pore using ordered and coupled conformational changes. Mol. Cell 6 (2000) 1233-42,

[29] L.A. Shepard, A.P. Heuck, B.D. Hamman, J. Rossjohn, M.W. Parker, K.R. Ryan, A.E. Johnson, R.K. Tweten. Identification of a membrane-spanning domain of the thiol-activated pore-forming toxin Clostridium perfringens perfringolysin O: an alpha-helical to beta-sheet transition identified by fluorescence spectroscopy. Biochemistry 37 (1998) 14563-74, 10.1021/bi981452f.

[30] B. Apellaniz, E. Rujas, P. Carravilla, J. Requejo-Isidro, N. Huarte, C. Domene, J.L. Nieva. Cholesterol-dependent membrane fusion induced by the gp41 membrane-proximal external region-transmembrane domain connection suggests a mechanism for broad HIV-1 neutralization. J. Virol. 88 (2014) 13367-77, 10.1128/JVI.02151-14.

[31] R. Abe, J.M. Caaveiro, H. Kozuka-Hata, M. Oyama, K. Tsumoto. Mapping ultra-weak protein-protein interactions between heme transporters of *Staphylococcus aureus*. J. Biol. Chem. 287 (2012) 16477-87, 10.1074/jbc.M112.346700.

[32] P. Evans. Scaling and assessment of data quality. Acta Crystallogr. D Biol. Crystallogr. 62 (2006) 72-82, 10.1107/S0907444905036693.

[33] A.J. McCoy, R.W. Grosse-Kunstleve, P.D. Adams, M.D. Winn, L.C. Storoni, R.J. Read. Phaser crystallographic software. J. Appl. Crystallogr. 40 (2007) 658-74, 10.1107/S0021889807021206.

[34] G.N. Murshudov, A.A. Vagin, E.J. Dodson. Refinement of macromolecular structures by the maximum-likelihood method. Acta Crystallogr. D Biol. Crystallogr. 53 (1997) 240-55, 10.1107/S0907444996012255.

[35] P. Emsley, B. Lohkamp, W.G. Scott, K. Cowtan. Features and development of Coot. Acta Crystallogr. D Biol. Crystallogr. 66 (2010) 486-501, 10.1107/S0907444910007493.

[36] R.A. Laskowski, M.W. Macarthur, D.S. Moss, J.M. Thornton. PROCHECK - A program to check the stereochemical quality of protein structures. J. Appl. Crystallogr. 26 (1993) 283-91, 10.1107/s0021889892009944.